Materials Advances

ROYAL SOCIETY OF CHEMISTRY

PAPER

View Article Online
View Journal | View Issue

Cite this: *Mater. Adv.*, 2025, 6, 4913

An efficient strategy for simultaneous gold deposition and obtention of hierarchical Au/TS-1 applied to liquid-phase propylene epoxidation†

Ignacio Centeno-Vega, *[a] Lorenzo José González-Rubio,[b] Cristina Megías-Sayago[a] and Svetlana Ivanova[b]

Received 6th March 2025,
Accepted 5th June 2025

DOI: 10.1039/d5ma00203f

rsc.li/materials-advances

A novel and straightforward one-step method has been developed for the controlled deposition of gold nanoparticles (AuNPs) with uniform diameters onto the titanosilicate (TS-1) zeolitic surface *via* a direct anionic exchange (DAE) approach. This innovative process simultaneously introduces auxiliary mesoporosity into the zeolite framework, overcoming critical limitations associated with traditional microporous catalysts, including diffusion constraints and rapid deactivation. The resultant hierarchical Au/TS-1 catalyst demonstrates remarkable enhancements in catalytic performance for the liquid-phase propylene epoxidation with H_2O_2 coupled with outstanding stability, a challenge that has long hindered the application of such materials. With its exceptional catalytic properties and simplified preparation procedure, this system represents a significant advancement in catalyst design. The developed material shows great potential for industrial applications and paves the way for the creation of next-generation catalysts essential for sustainable development.

1. Introduction

Plastic materials have undergone exponential growth in production during the last decades due to their ease and low cost of manufacturing in addition to their versatility. In 2019, it was estimated that worldwide industrial production of plastics reached a value of 460 million tons,[1] with the majority (around 99%) coming from fossil-fuel-based resources.[2] In our current society these materials are truly essential and it would be almost impossible to imagine a world without their presence so, evidently, this industry will keep growing every year, with the annual demand of these materials being expected to triple by 2060 to keep up with population increase.[3] Of the total current synthetic plastic production, the packaging sector represents the largest plastic market, accounting for 40% of all the polymers generated by this industry.[2,4] This industry is currently designed on the basis of a linear economy, founded on the single-usage of plastics which are readily discarded afterwards, producing an excessive amount of waste that has not been designed to be easily recyclable. Therefore, the industry needs to shift to a circular economy and use the mentioned materials, designing and producing them from renewable feedstocks while maintaining their properties for the corresponding purpose, resulting in the reduction of the associated carbon footprint, which was estimated to be 860 million tons in 2019.[4] In this sector, polyethylene terephthalate (commonly referred to as PET) is of great relevance for the bottling of various beverages, accounting for 7% of global plastic production.[2,5,6] Although it is a recyclable material, its production involves non-renewable fossil feedstocks, in addition to being a material that does not decompose easily when disposed of in the environment, thus contributing to soil and water pollution.

A sustainable alternative to petroleum-derived polymers is polypropylene furanoate (PPF), which stands out as a competitive and bio-renewable option. PPF is a new generation plastic with matching properties to PET (even outperforming it in certain aspects such as improved barrier properties for O_2 and CO_2),[7–10] which can be obtained through the polymerization of 2,5-furandicarboxylic acid (an oxidation product of the platform chemical HMF derived from biomass) and propylene glycol. A sustainable approach for the production of glycol is to use plastic waste (such as polyethylene and polypropylene) as starting feedstock, an inexpensive source of hydrocarbon chains which has proven to be exceptionally promising for the selective obtention of propylene through cutting-edge metathesis processes.[11–14] Subsequently through its corresponding epoxidation and posterior ring-opening hydration, the respective diol could be obtained starting from propylene. This way a truly circular process could

[a] *Departamento de Química Inorgánica, Instituto de Investigaciones Químicas and Centro de Innovación en Química Avanzada (ORFEO-CINQA), Centro mixto CSIC-Universidad de Sevilla, 41092 Sevilla, Spain. E-mail: icenteno@us.es*
[b] *Departamento de Química Inorgánica e Instituto de Ciencia de Materiales de Sevilla, Centro Mixto CSIC-Universidad de Sevilla, 41092 Sevilla, Spain*

† Electronic supplementary information (ESI) available. See DOI: https://doi.org/10.1039/d5ma00203f

be developed, reducing the amount of fossil-derived plastic waste found in the environment by replacing it with its bio-based counterpart PPF.

The traditional industrial routes for propylene oxide (PO) synthesis, namely chlorohydrin and hydroperoxide processes, are efficient but present significant environmental challenges. In the past years, an environmentally benign process known as the HPPO (hydrogen peroxide propylene oxide) process has risen as the most promising alternative due to the obtention of water as the sole by-product and the use of hydrogen peroxide as a green oxidant. However, methanol is also employed in the process to increase propylene solubility and because of the mixture of solvents employed, the resulting epoxide is susceptible to suffer from ring-opening reactions due to the nucleophilic attack of the solvent, whether methanol or water. This way, the corresponding glycol can be obtained through the hydrolysis of the epoxide, while other products can also be found such as monomethyl ethers of propylene glycol, 1-methoxypropan-2-ol (1M2P) and 2-methoxypropan-1-ol (2M1P), highlighting the need for the development of a highly selective catalyst in this transformation (Fig. 1). In this process, titanium silicalite-1 (TS-1), a microporous zeolite with an MFI-type structure, is used as a catalyst due to the presence of tetrahedrally coordinated Ti(IV) sites within the TS-1 framework which are capable of activating H_2O_2. Despite its remarkable activity in the oxidation of organic substrates, TS-1 suffers from limitations in liquid-phase reactions because of its purely microporous structure, restricting the diffusion of larger molecules thus hindering its catalytic efficiency, in addition to poor stability and rapid deactivation due to pore blockage and carbon deposition. To address these limitations, zeolites can be endowed with a hierarchical structure through the creation of mesopores alongside the intrinsic micropores, allowing better access to active sites and avoiding their deactivation by pore-blockage or carbon deposition.

In this study, several TS-1 catalysts with different Si/Ti ratios have been synthesized and subsequently used as support for the deposition of gold nanoparticles through a direct anionic exchange (DAE) procedure which simultaneously introduces auxiliary mesoporosity in the zeolitic framework and increases the number of catalytically active tetrahedral Ti sites in the silicalite surface. The resulting TS-1 and Au/TS-1 catalysts' performance has been studied in the H_2O_2-assisted liquid phase epoxidation of propylene and in the case of the gold-containing catalysts they were compared to their conventional counterparts prepared by incipient wetness impregnation and colloidal deposition. Key parameters influencing catalytic activity and selectivity were systematically analyzed, such as gold loading, Si/Ti molar ratio and presence of auxiliary mesoporosity. Additionally, catalyst stability was assessed over multiple consecutive runs.

2. Experimental section

2.1. Materials

For the synthesis of TS-1 zeolites with different Si/Ti molar ratios the following precursors were employed: tetraethyl orthosilicate (TEOS, ≥98%, Sigma-Aldrich) as a Si source, tetraethyl orthotitanate (TEOT, ≥97%, Sigma-Aldrich) as a Ti source and tetrapropylammonium hydroxide (TPAOH, 1 M aqueous solution, Sigma-Aldrich) as a structure directing agent. In the posterior deposition of gold nanoparticles $HAuCl_4$ (Johnson Matthey) was employed as an Au precursor and NH_3 (Sigma-Aldrich) was used for the DAE procedure. For the preparation of the Au/TS-1 catalyst through colloidal deposition polyvinyl alcohol (PVA, Sigma Aldrich) and $NaBH_4$ (Alfa-Aesar) were required.

For the liquid-phase catalytic epoxidation tests the following reagents were used: hydrogen peroxide (H_2O_2 30% wt Sigma-Aldrich), methanol (≥99.9%, Merck Millipore) and propylene (99.95%, Linde). Additionally, for the residual hydrogen peroxide concentration titration $KMnO_4$ (≥99%, Panreac) and $Na_2C_2O_4$ (≥99.5%, Sigma-Aldrich) were employed.

2.2. Preparation of TS-1 catalysts

TS-1 zeolites employed in this research have been synthesized following the two-step hydrolysis procedure described by

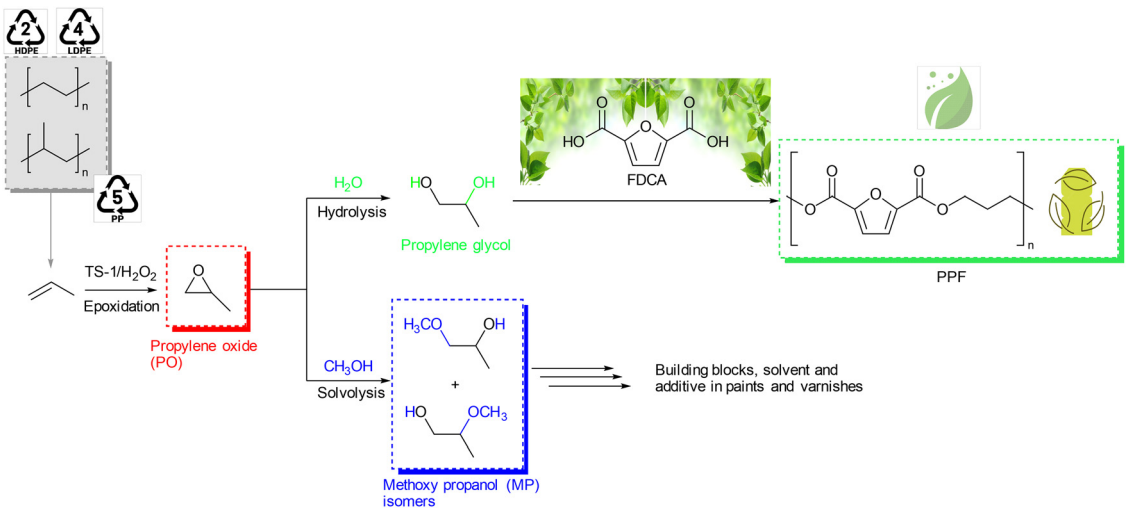

Fig. 1 Obtention of propylene glycol through HPPO route and posterior polymerization with FDCA to produce PEF.

Deng *et al.*[15] Initially, a mixture of the entirety of TEOT (0.375–1.5 mmol) to be employed in the reaction and a third of the total amount of TEOS (25 mmol) is prepared. This mixture is added dropwise into a 1 M TPAOH solution under constant stirring at room temperature. The resulting gel is heated at 323 K for 30 min in a hydrolysis step and subsequently temperature is increased to 353 K for another 30 minutes in order to promote alcohol removal by evaporation, obtaining a sol with molar composition: $1.0SiO_2$:(0.015–0.06)TiO_2:0.7TPAOH:$38H_2O$.

After cooling down, the remaining TEOS (50 mmol) is added to the previously prepared sol dropwise under continuous stirring. Moreover, 20 mL of distilled water is poured into the vial to favor hydrolysis and replenish the lost volume in the system. The heating steps for hydrolysis and alcohol removal are repeated under the same conditions as the previous step. The resulting mixture is transferred to a stainless-steel autoclave where its crystallization will take place for 48 hours at 443 K. The obtained solid is recovered and washed several times through centrifugation. Ultimately, said whitish dust is dried overnight at 373 K and calcined at 873 K for 6 hours to remove the remaining organic species present in the framework's pores. The resulting zeolites are designated as ''TS_X'' being X the molar ratio Si/Ti for each sample.

2.3. Au nanoparticle deposition over TS-1

For the deposition of gold nanoparticles over the surface of previously prepared titanium silicalite a direct anionic exchange (DAE) procedure assisted by NH_3 was followed.[16,17] Deposition of gold (1% wt) in the several zeolitic supports was achieved through their addition to a $HAuCl_4$ aqueous solution (10^{-4} M) at 343 K under constant stirring. Once mixed, the solution was aged for 20 minutes before the addition of 20 mL NH_3. The resulting slurry was finally filtered, washed with water and dried at 373 K overnight. Subsequently, samples are reduced at 423 K for 1 hour under a 4% H_2 flow and ultimately calcined at 573 K for 1 hour in an 8% O_2 flow (both balances performed with N_2 as inert gas). The resulting zeolitic catalysts are labeled ''Au/TS_X'' being ''X'' once again the molar Si/Ti ratio of each sample.

2.3.1 Safety note. Ammonia reaction with a gold precursor solution can lead to the formation of potentially explosive gold ammonia complexes, known as ''fulminating gold''. For safety reasons a highly diluted gold precursor solution is employed. Anyway, this preparation procedure is not dangerous when the gold complexes are strongly attached to the support by the DAE method.

Moreover, conventional Au/TS-1 catalysts were prepared by incipient wetness impregnation and colloidal deposition for comparison. For the colloidal method, a 5×10^{-4} M solution of $HAuCl_4$ was employed upon which was added a PVA solution (1% wt aqueous solution) in order to reach a PVA : Au weight ratio of 0.85. After 20 minutes of stirring, the required amount of a freshly prepared 0.1 M $NaBH_4$ solution was poured until achieving a $NaBH_4$: Au molar ratio equal to 10. Upon additional 20 minutes of stirring, the resulting colloid was put in contact with the adequate amount of TS-1 in order to have a nominal gold loading of 1 wt%. The obtained mixture was centrifuged at 15 000 rpm with the aim to successfully anchor the entirety of the colloidal gold into the support. Subsequently, the sample was filtered, dried overnight at 100 °C and finally calcined at 300 °C for 2 h in static air, obtaining the catalyst labeled as Au/TS_30-C (C stands for ''colloidal'').[18] The sample prepared by incipient wetness impregnation was named Au/TS_30-I (I stands for ''impregnation'').

2.4. Catalytic tests

Catalytic activity of the previously synthesized TS_X zeolites and their gold-modified analogues (Au/TS_X) was analyzed in the liquid phase epoxidation of propylene. These trials were carried out in a 25 mL Parr autoclave reactor, equipped with mechanical stirring in addition to a precise temperature and precision control.

In a typical run 150 mg catalyst, 10 mL methanol and 2.58 mL H_2O_2 (30 mmol, 35% wt) were fed into the reactor. Once the reactor has been sealed and checked for leaks with N_2, it is purged twice with propylene to replace internal air. Reaction was performed at 323 K for 2 hours with constant stirring under a propylene pressure of 0.4 MPa. After this period, the reactor is cooled down with an ice bath and a reaction sample is taken through microfiltration for its posterior product identification by gas chromatography in a Shimadzu GC-2010 chromatograph equipped with an Sh-rxi-5ms column coupled to a Shimadzu GCMS-TQ8040 mass spectrometer. Product quantification was performed in a Shimadzu GC-2010 Pro chromatograph equipped with the same column and a flame ionization detector (FID). In order to be able to carry out the quantification, the response factors of each compound had been previously determined using acetonitrile as an internal standard. Residual H_2O_2 concentration in the liquid phase is determined by indirect permanganometric titration, through its previous standardization with sodium oxalate. The catalytic performance was evaluated using the following expressions (eqn (1)–(4)):

$$\text{PO yield} = \frac{n_{\text{PO}}}{n^0_{\text{Propylene}}} \times 100\% \quad (1)$$

$$\text{PO select} = \frac{n_{\text{PO}}}{n_{\text{PO}} + n_{\text{PG}} + n_{\text{MP}}} \times 100\% \quad (2)$$

$$\text{H}_2\text{O}_2 \text{ conv.} = \frac{n^0_{\text{H}_2\text{O}_2} - n_{\text{H}_2\text{O}_2}}{n^0_{\text{H}_2\text{O}_2}} \times 100\% \quad (3)$$

$$\text{H}_2\text{O}_2 \text{ eff.} = \frac{n_{\text{PO}} + n_{\text{PG}} + n_{\text{MP}}}{n^0_{\text{H}_2\text{O}_2} - n_{\text{H}_2\text{O}_2}} \times 100\% \quad (4)$$

where n_{PO}, n_{PG} and n_{MP} denote the molar content of PO, PG and MP, respectively. Eqn (1) and (2) were additionally employed to determine PG and MP yield and selectivity by exchanging the numerator in the expression. Moreover, $n^0_{\text{H}_2\text{O}_2}$ and $n_{\text{H}_2\text{O}_2}$ represent the initial and final molar amount of hydrogen peroxide, respectively.

2.5. Characterization

XRD measurements were performed in an X'Pert Pro PANalytical diffractometer equipped with a Cu anode and working at 45 kV/40 mA. Diffractograms were registered in the 5 to 90° 2θ range with a 0.05° step and 300 seconds of acquisition time. Structure and phase determination were conducted in comparison to the database PDF2 ICDD2000 (Powder Diffraction File 2 International Center for Diffraction Data).

Catalysts' textural properties were determined through N_2 physisorption at 77 K in a Micromeritics Tristar II equipment. Previous to the adsorption, samples were degassed at 573 K for 4 hours in a Micromeritics 061 VacPrep vacuum system. BET method was employed to determine specific surface area through the adsorption isotherms and pore size distribution was calculated according to the BJH method.

Inductively couple plasma optical emission spectroscopy (ICP-OES) was employed in order to perform the elemental and quantitative analysis of the synthesized catalysts. Si, Ti and Au content was determined using an iCAP 7200 ICP-OES Duo (ThermoFisher Scientific) spectrometer. To carry out the measurements samples were previously digested in an acid media employing a microwave digestion system ETHOS EASY (Milestone).

TS-1 zeolite particles were visualized through scanning electron microscopy (SEM) in an S4800 Hitachi equipment with a 200 kV acceleration potential. After gold nanoparticles' deposition in the zeolitic surface, samples were analyzed in a high-resolution transmission electron microscope (HR-TEM) JEOL 2100Plus (200 kV) equipped with a LaB_6 filament. Digital images were taken with a CCD camera (Gatan) with the samples being deposited over a copper grid.

X-Ray photoelectron spectroscopy (XPS) experiments were performed in a PHOIBOS-100 spectrometer with a nonmonochromatic Al-Kα (1486.6 eV). Low resolution survey spectra were obtained with a pass energy = 50 eV, while high energy resolution spectra of detected elements (*i.e.*, Au4f, Ti2p, C1s, O1p, and Si2p) were obtained with a pass energy = 35 eV. The analytical chamber operates at ultra-high vacuum at around 10^{-9} torr pressure. The XPS spectra are recorded at room temperature and referenced to the C1s, adjusted to 284.6 eV and fitted using CasaXPS software with Gaussian–Lorentzian peak shapes and Shirley baselines.

3. Results and discussion

3.1. Characterization of TS-1 and Au/TS-1 catalysts

3.1.1 X-Ray diffraction. X-Ray diffraction patterns of the synthesized TS-1 and Au/TS-1 catalysts with different Si/Ti atomic ratios are displayed in Fig. 2. All samples exhibit the 5 characteristic diffraction peaks typically assigned to a MFI-type zeolite structure, namely 2θ = 7.9°, 8.8°, 23.1°, 23.9° and 24.4°.[19–23] Additionally, no peak can be seen at 25.4°, characteristic of the anatase crystalline phase corresponding to the formation of extra reticular TiO_2, suggesting a satisfactory introduction of the entirety of the titanium species in the zeolitic framework without the formation of extra-framework anatase.[22,24] In the gold-containing samples it can be observed how the diffractograms exhibit the same pattern, indicating that the structure is maintained after metal loading, hardly affecting the initial silicalite properties. Moreover, diffractograms of catalysts prepared through incipient wetness impregnation and colloidal method are compared to the ones obtained by the DAE procedure (Fig. S1, ESI†), exhibiting the same pattern. No peak can be assigned to the characteristic diffraction of Au (2θ = 38.1°) in the DAE and colloidal catalysts corresponding to its (111) crystal plane.[21,22,25] This fact highlights the obtention of highly dispersed gold nanoparticles throughout the zeolitic surface, successfully avoiding its aggregation during the preparation procedure. However, gold deposition through incipient wetness impregnation results in larger particles since its corresponding diffraction peak is detected (Fig. S2, ESI†). The samples' crystallinity is maintained as Ti content is increased, judging by the equivalent relative intensity of the MFI-type peaks, and thus it is safe to state that the introduction of Ti atoms does not have a significant effect on the MFI-type structure of the studied samples or their crystallinity.[24,26,27]

3.1.2 N_2-Physical adsorption. N_2 adsorption isotherms of the synthesized catalysts are displayed in Fig. 3. These graphic representations exhibit the shape of a combined isotherm of type I and type IV according to IUPAC, a characteristic feature of

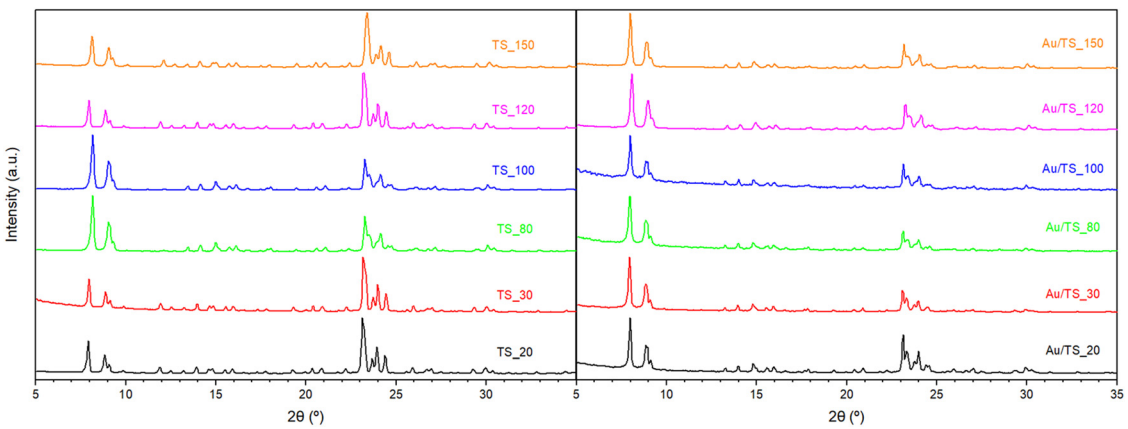

Fig. 2 XRD patterns of the synthesized TS_X and Au/TS_X catalysts.

a hierarchical porous material that presents both micro- and mesopores.[21,28–33] The presence of micropores can be confirmed by the sharp increase in the quantity adsorbed at low relative pressures ($P/P_0 < 0.1$). Likewise, mesopores are evidenced by a similar increase at higher relative pressures in addition to an evident H4 hysteresis loop in the P/P_0 0.2–1.0 range. In the TS_X catalysts, the narrow hysteresis loop arises as a result of the interparticle spacing. However, deposition of gold produces a steeper increase at high relative pressures which can be attributed to a promoted formation of mesopores during the DAE procedure.

Tables 1 and 2 display the textural properties of the several catalysts studied in this research. In general terms, it can be affirmed that as the Ti content is increased the BET surface area is also enhanced due to silicalite unit cell expansion because of the introduction of titanium species in the MFI-type structure, as previously reported in the literature.[24,26,27] All TS_X samples exhibit similar pore volume; however, it can be seen how for the ones with the highest Ti content the mesopore proportion is increased to the detriment of micropores (Table 1, Samples TS_20 and TS_30). After gold deposition, all catalysts exhibit increased surface area, pore volume and pore size in comparison to their pure titanosilicate counterparts. During the deposition process, the change in the pH values to which the zeolite is subjected due to the presence of NH_3 may cause the titanosilicate to undergo ammonia-assisted surface etching, further enhancing its surface area due to the formation of additional porosity. Aforementioned auxiliary porosity introduced in the samples during the gold deposition procedure is made up solely of mesopores, since it can be seen how equivalent samples show the same (or even lower, due to micropore blockage by the gold nanoparticles) values of microporosity while its mesoporosity is greatly enhanced after the DAE procedure (*e.g.* Table 1, entry TS_20 *vs.* Table 2, entry Au/TS_20), as illustrated in Fig. 4 displaying the change in pore size distribution after the deposition of Au nanoparticles. This way, we can confirm the successful controlled introduction of uniform intracrystalline mesopores of *ca.* 4 nm width in the TS-1 samples, achieving an enhanced mesoporosity at the expense of microporosity.

Table 1 Textural properties of representative TS_X samples with different Si/Ti molar ratios

	Surface area ($m^2\ g^{-1}$)			Pore volume ($cm^3\ g^{-1}$)			
Sample	S_{BET}	S_{micro}	S_{BJH}	V_T	V_{micro}	V_{meso}	Pore size (Å)
TS_20	389	110	279	0.21	0.05	0.16	21.68
TS_30	417	142	275	0.23	0.06	0.17	21.85
TS_80	350	259	91	0.21	0.12	0.09	23.70
TS_100	351	250	101	0.22	0.12	0.10	24.90

Table 2 Textural properties of representative Au/TS_X samples with different Si/Ti molar ratios

	Surface area ($m^2\ g^{-1}$)			Pore volume ($cm^3\ g^{-1}$)			
Sample	S_{BET}	S_{micro}	S_{BJH}	V_T	V_{micro}	V_{meso}	Pore size (Å)
Au/TS_20	429	130	299	0.34	0.05	0.29	31.48
Au/TS_30	449	127	322	0.34	0.05	0.29	30.71
Au/TS_80	434	186	248	0.41	0.09	0.32	38.14
Au/TS_100	444	204	240	0.42	0.10	0.32	38.04

3.1.3 Electron microscopies. Fig. 5 shows SEM images of two TS-1 catalysts prepared with different Si/Ti ratios. The TS-1 particles exhibit a blueberry-like morphology with an average size of *ca.* 180 nm. It can be seen how the surface of TS_20 particles is rougher than TS_80 likely owing to the precipitation of small amounts of extra-reticular TiO_2 in the form of anatase, while the lower Ti-containing sample has incorporated successfully all the Ti species in the framework resulting in a smoother surface. Upon gold deposition it is quite obvious that the change in the surface properties of both samples, being able to observe a greater number of pores, in addition to being larger in size, in accordance with the textural properties previously determined by N_2 physisorption. Furthermore, in the TS_20 samples, it can be seen how its gold-containing counterpart exhibits a smoother surface due to the "cleansing" effect that takes place due to the presence of ammonia, dissolving extra-reticular titanium species which has been reported to be beneficial for epoxidation activity since those species decompose hydrogen peroxide reducing the

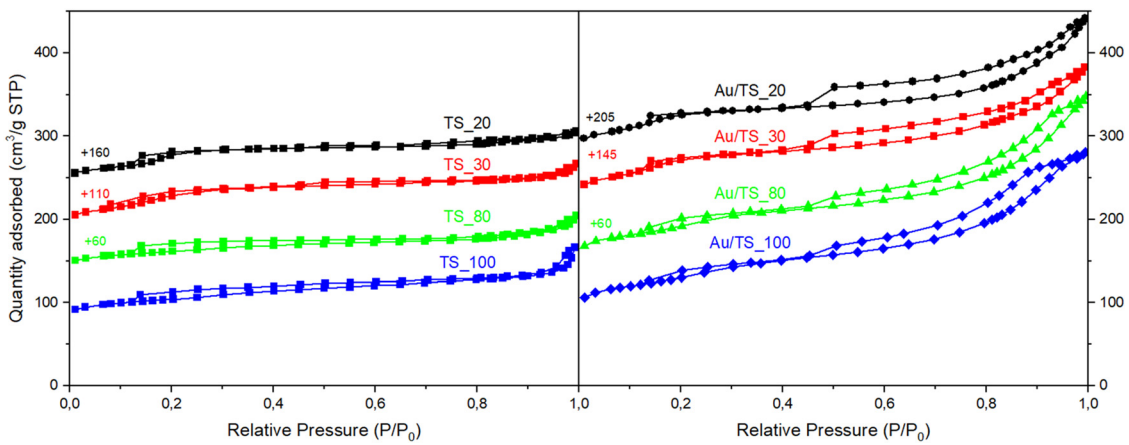

Fig. 3 N_2 adsorption–desorption isotherms at 77 K for the TS_X and Au/TS_X catalysts.

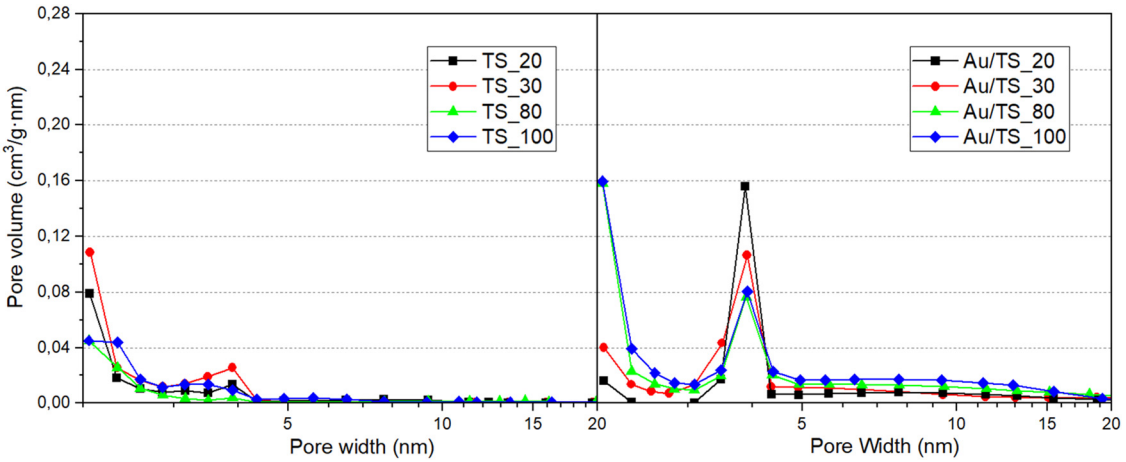

Fig. 4 Pore size distribution of representative TS_X and Au/TS_X samples.

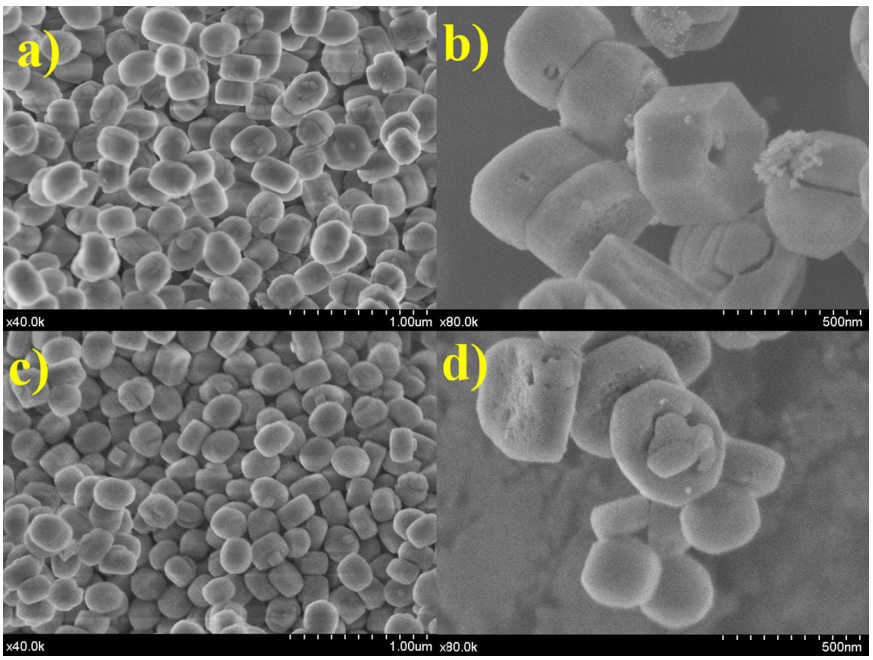

Fig. 5 SEM images of synthesized catalyst (a) TS_20 and (b) after its corresponding gold deposition; (c) synthesized TS_80 and (d) after its corresponding gold deposition.

efficiency in the process.[19,34] This dissolution step increases the proportion of surface tetrahedrally-coordinated Ti sites through the removal of extra-framework octahedral species, achieving a more efficient catalyst not only by enhancing the number of active sites per silicalite weight but also by improving the reactants' accessibility to said sites by the enlargement of the pores and shortened diffusion path lengths, avoiding mass transfer issues and lowering the probability of secondary reactions taking place.[29,32–38] In addition, this dissolution process leads to a gradually decreased amount of terminal silanol groups (Si–OH), improving the hydrophobicity of the catalyst's surface and favoring the desorption of PO molecules, restraining the deposition of carbonaceous species and self-poisoning of the active sites.[33,36,39,40]

In Fig. 6 it can be observed a representative TEM image taken with a HAADF detector of both Au/TS_X catalysts previously analyzed by SEM along with their respective size distribution histogram for the Au nanoparticles. This way it is evidenced once again by the additional mesoporous structure that has been induced during the deposition procedure and etching treatment, resulting in wider pores that penetrate deep into the particle structure. Regarding the gold nanoparticles, it can be stated that they have been introduced in a controlled way, obtaining highly dispersed particles throughout the surface with a narrow size range that obeys a normal distribution.

3.1.4 Elemental analysis. Table 3 displays the elemental quantification experimental values obtained by ICP of the

several catalysts studied, along with their average Au nanoparticle size. In general terms, the targeted Si/Ti ratios are quite close to the nominal values, which were arduous to achieve due to the challenging introduction of Ti species into the MFI framework. Regarding gold loading, the obtained experimental values are once again satisfactorily close to the nominal value of 1% wt in the samples with a high titanium content (low Si/Ti ratio). However, it can be noticed that the gold content gradually decreases as the titanium content diminishes, deviating significantly from the nominal value especially in the Au/TS_150 sample. This fact can be attributed to the modification of the support isoelectric point (IEP) by the introduction of Ti, which results in the obtention of a more positively charged surface with higher IEP values. Therefore, due to the inherent characteristics of the DAE method, these positively charged surfaces of the Ti-rich samples would adsorb gold anionic species more favorably than the samples with a high Si/Ti ratio, achieving complete gold deposition.[41]

3.1.5 X-Ray photoelectron spectroscopy (XPS). The general XPS spectra of the TS_30 and Au/TS_30 samples are summarized in Fig. S3 (ESI†). Overall, the deposition of gold does not provoke any significant changes in the general scan except for the Au presence for the Au/TS-30 sample.

A detailed analysis of the Ti 2p high resolution spectra (Fig. 7) reveals two doublets, the one at 458.2 ± 0.2 eV assigned to octahedral Ti like the one present in titania and the second at 460.2 ± 0.2 eV assigned to tetrahedral Ti incorporated to the zeolite framework.[42–44]

Table 3 Elemental quantification and average gold nanoparticle size of studied Au/TS_X catalysts

Catalyst	Si/Ti (ICP)	% Au wt (ICP)	Au NPs diameter (nm)
Au/TS_20	23.8	1.13	6.88 ± 3.50
Au/TS_30	25.4	0.92	5.72 ± 3.01
Au/TS_80	81.4	0.96	5.23 ± 2.40
Au/TS_100	108.7	1.07	5.16 ± 2.06
Au/TS_120	115.4	0.84	3.66 ± 1.50
Au/TS_150	149.1	0.55	5.67 ± 2.60

While the tetrahedral coordination refers to titanium accommodated into the silica framework the octahedral coordination derives either from the conversion of tetracoordinated titanium located at the surface to octahedrally coordinated through reaction with water or to the segregation of TiO_2 during TS-1 synthesis. Considering the lower Si/Ti ratio of this sample one can presume that an important part of Ti is segregated as octahedral Ti. The fresh TS-30 sample shows a Ti_{Oh}/Ti_{Td} ratio of 2 which diminishes after the gold deposition (Table S1, ESI†) due to the decreased TiO_2 contribution after ammonia treatment. On the other hand, the surface Si/Ti ratio

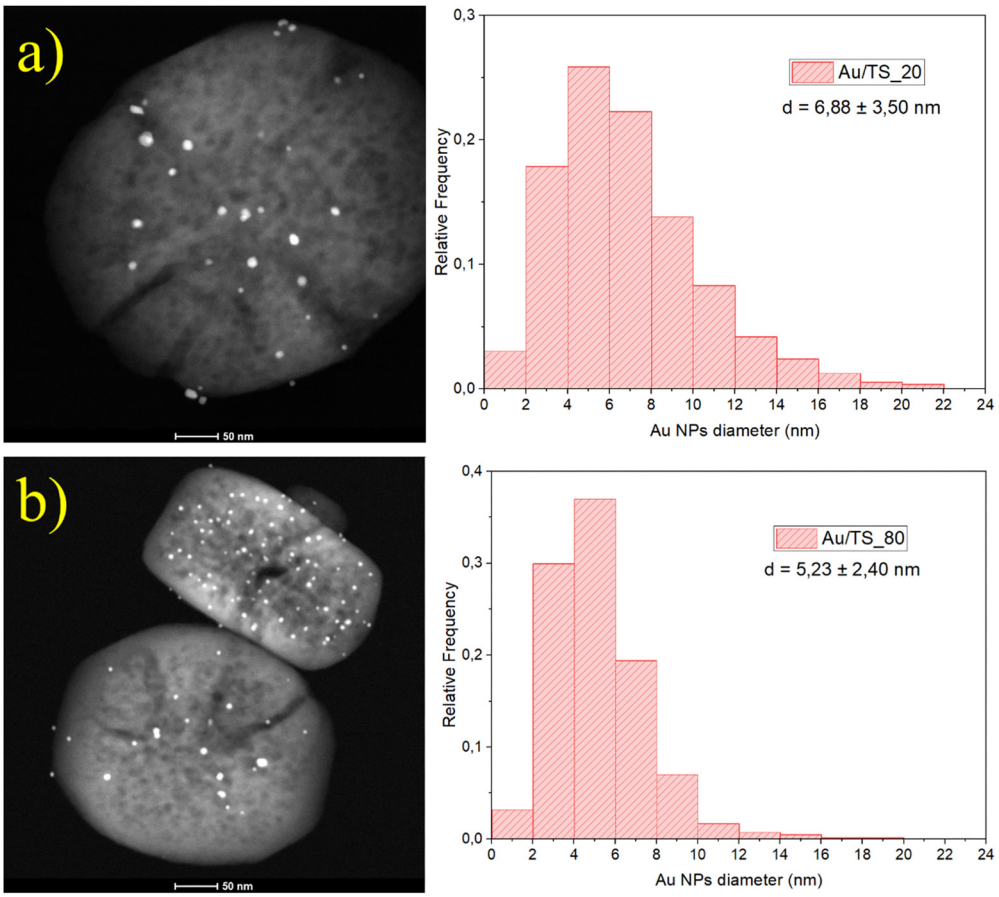

Fig. 6 Representative TEM image with HAADF detector of (a) Au/TS_20 and (b) Au/TS_80 catalysts and their respective gold nanoparticles size-distribution histogram.

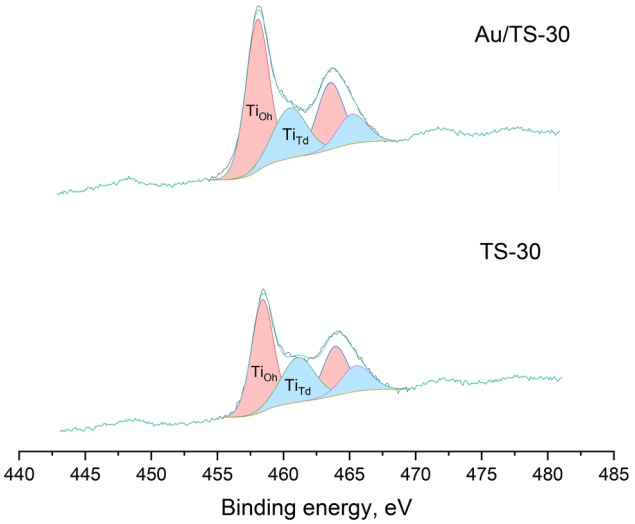

Fig. 7 Ti 2p high resolution XPS spectra of TS_30 and Au/TS_30 samples.

is close to the measured by ICP and increases after gold deposition due to the decrease of the Ti surface composition owing to the ammonia-assisted etching, being the Ti_{Oh} loss much more important than that of Ti_{Td}, resulting in an increase in the number of catalytically active sites relative to silicalite weight.

As for gold, the surface composition of the Au/TS_30 sample indicates a very good dispersion and pure metallic state (Fig. S4, ESI†).

3.2. Propylene epoxidation

3.2.1 Catalytic performance. Product yields and selectivities with the different TS_X and Au/TS_X catalysts in the propylene epoxidation reaction are included in Tables S2–S4 (ESI†) and represented in Fig. 8 along with hydrogen peroxide conversion and efficiency. All TS-1 catalysts exhibit similar product distribution, being propylene oxide (PO) the major product in every case, with selectivity values exceeding 95% at every instance and obtaining only a minor amount of PG and MP as side-products. Despite this outstanding selectivity, the achieved yields are quite far from being satisfactory, reaching only an appreciable propylene conversion with the higher Ti loading catalysts. With the introduction of gold, a drastic shift can be observed in the catalytic properties of the system. In general terms, every catalyst exhibits higher yields upon gold deposition due to an increased propylene conversion.

For the zeolites with the lower Ti content the overall propylene conversion and PO yield are still rather low even though they still show a remarkable selectivity. As the Si/Ti ratio is decreased, the PO yield is greatly enhanced at the cost of sacrificing its initial selectivity. Catalyst Au/TS_30 achieves a PO yield close to 50% while still maintaining its selectivity value proximate to 90%, reaching a compromise between both parameters and resulting in the most promising catalyst for this transformation due to its minority production of secondary compounds. Increasing the Ti content even further results in a slight improvement of PO yield, displaying an accurate exponential relationship between the obtained PO yield and the Si/Ti ratio of the studied catalysts, as shown in Fig. S5 (ESI†). This increase in activity noticeably enhances MP production as well, as a result of using methanol as a solvent in the process.

Usage of water : methanol mixtures could shift the catalyst selectivity towards the production of PG, leading to an increased yield of this compound and resulting in a promising and greener process for the *in situ* production of bio-based polymers such as PPF. Besides the drop in selectivity with this catalyst we can highlight its outstanding performance in the activation of propylene, being the catalyst that provides the highest conversion values.

As for the use of hydrogen peroxide as an oxidant, it is evidenced that the presence of gold nanoparticles in the catalyst enhances both the conversion and efficiency in its usage by promoting H_2O_2 activation. This way, the synergistic interaction between the gold nanoparticles and the Ti active sites can be confirmed, resulting in higher yields for PO formation in this transformation.[45]

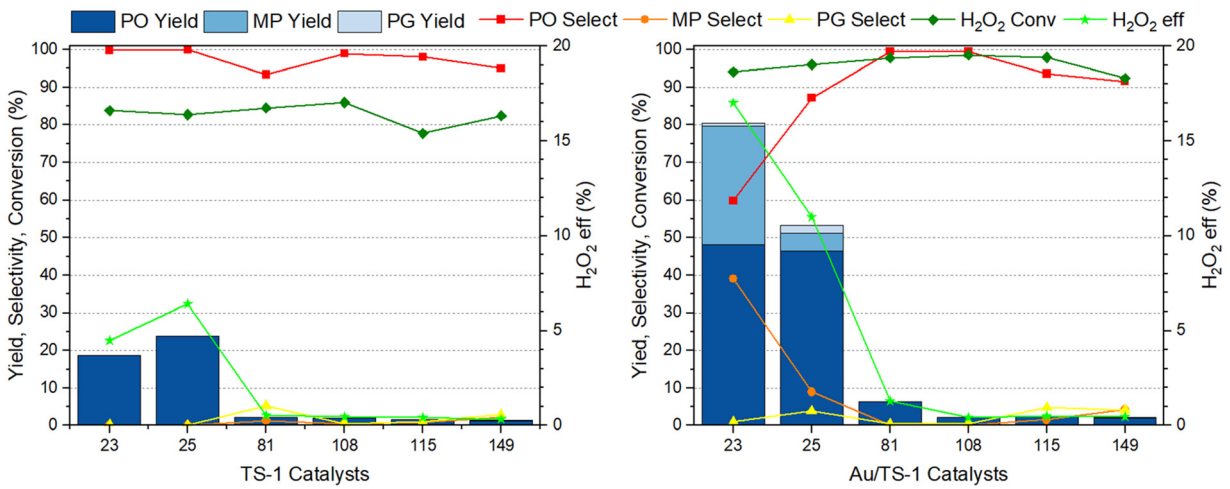

Fig. 8 Product distribution in propylene epoxidation reaction with TS_X and Au/TS_X catalysts. Reaction conditions: 150 mg catalyst, 10 mL methanol, 2.58 mL H_2O_2 35% wt (30 mmol) and 4 bar propylene for 2 hours at 50 °C.

Catalysts prepared with the DAE procedure and their counterparts obtained by impregnation and colloidal deposition are compared in Table S4 (ESI†) where their catalytic performances are summarized and it can be observed that the DAE procedure stands out with the highest PO yield. Gold deposition through other methods not only does not achieve the same values as DAE but also worsens the catalytic activity of bare TS_30, promoting the formation of side-products, mainly MP, at the expense of reduced PO yields. Gold nanoparticle size can be ruled out as the possible explanation for this loss of selectivity, since colloidal deposition (Au/TS_30-C) achieves small particles of controlled-size that are outperformed by its DAE equivalent. Despite the lower selectivities, gold presence improves propylene conversion in every case through enhanced H_2O_2 activation. Therefore, it can be stated with certainty that the gold deposition method plays a crucial role in enhancing this transformation, not only by facilitating propylene conversion and increasing oxidant utilization efficiency, but also by tailoring TS-1 inherent textural properties in a simple deposition procedure. In this way, enlarged pore channels are obtained, favoring mass transfer and diffusion processes, which in addition to the improved hydrophobicity of the resulting surface, reduced acid strength and the exposure of a larger number of active sites (tetrahedral Ti species, as evidenced by XPS analysis) translates into an enhanced propylene conversion and PO yield.[29,31,32,39,40,46,47]

Activity studies were also carried out over different reaction times in order to gather a better insight into Au/TS_30 catalyst's performance, as shown in Fig. 9. It can be observed how for an initial reaction time of 30 minutes PO is exclusively formed, highlighting the outstanding selectivity achieved with this catalyst when propylene is the only compound present in the media. As the reaction time is increased to 2 hours and PO starts accumulating in the reactor, the extent to which ring-opening reactions take place is enhanced, detecting noticeable quantities of PG and MP, thus resulting in a decline of PO selectivity. Further extending the reaction time to 4 hours does not lead to the conversion of any additional propylene, suggesting that at this point only the previously formed PO is the reactive species and exclusively ring-opening reactions are taking place, diminishing the resulting PO yield. This fact can be attributed to pore-blocking deactivation by PO physisorption as a plausible mechanism, in addition to the selective chemical deactivation of Ti active sites through PO chemisorption forming a bidentate ether species among Ti–OH and adjacent Si–OH groups.[48,49]

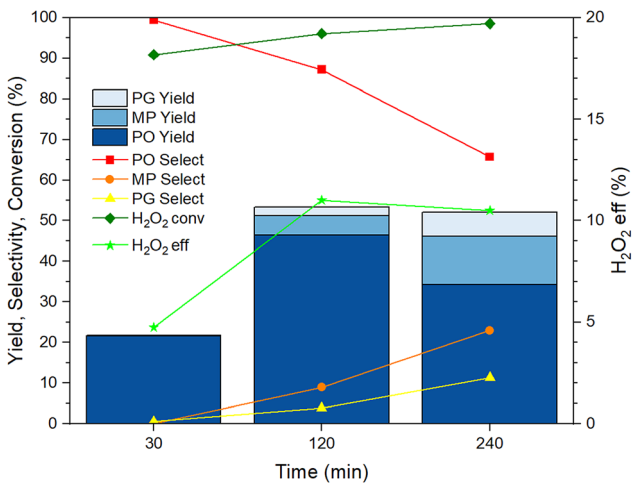

Fig. 9 Product distribution evolution over time in propylene epoxidation reaction with Au/TS_30 catalyst. Reaction conditions: 150 mg catalyst, 10 mL methanol, 2.58 mL H_2O_2 35% wt (30 mmol) and 4 bar propylene at 50 °C for different time periods.

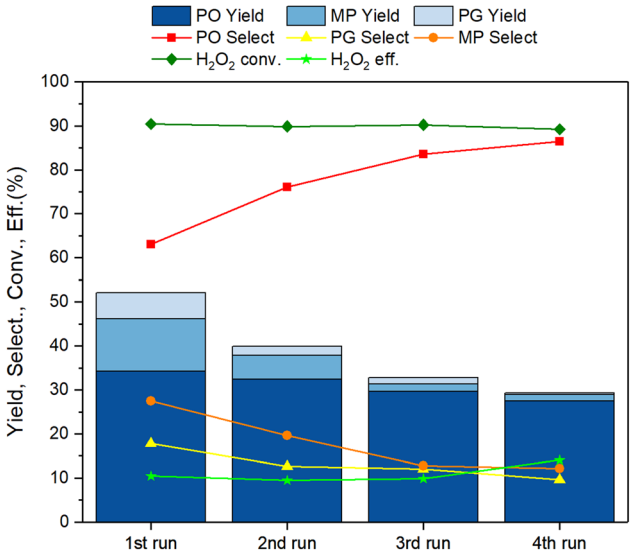

Fig. 10 Recyclability test in the propylene epoxidation reaction with the Au/TS_30 catalyst over 4 consecutive runs. Reaction conditions: 150 mg catalyst, 10 mL methanol, 2.58 mL H_2O_2 35 wt% (30 mmol) and 4 bar propylene for 4 hours at 50 °C.

3.2.2 Reusability tests. In order to verify catalyst stability, recyclability tests were performed with Au/TS_30 in propylene epoxidation over 4 different runs. The catalyst was recovered simply through filtering and drying, with no regeneration cycles in order to subject the catalyst to harsher conditions, as well as increasing reaction time to 4 hours for the same reason. The obtained results are shown in Fig. 10. Throughout the runs it can be seen how PO yield and H_2O_2 conversion are maintained nearly constant but ring-opening reactions are disfavored, resulting in a negligible amount of MP and PG obtained in the final run. Therefore, far from observing the deactivation of the catalyst after working for 960 minutes, it was noticed that the catalyst maintained its activity satisfactorily, even reaching higher PO selectivity values in the final run, as well as a better efficiency in the utilization of hydrogen peroxide. As confirmed by TEM analysis, there does not appear to occur a significant gold nanoparticle aggregation after the performed recyclability tests (Fig. 11). This way, we can assure the development of a truly and exceptionally stable Au/TS-1 catalyst, overcoming the main drawback characteristic of these catalysts as has been previously described in the literature.[20,37,40,50–52] Aforementioned outstanding stability could be attributed to the hierarchical structure of the catalysts, which inhibits carbon deposition and avoids pore

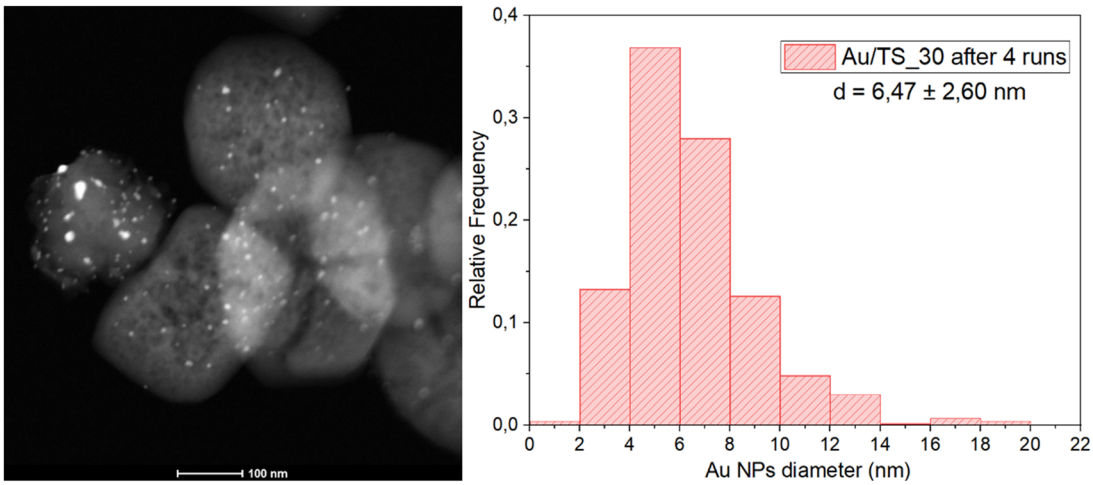

Fig. 11 Representative TEM image with HAADF detector of the Au/TS_30 catalyst after 4 epoxidation runs and its respective gold nanoparticle size-distribution histogram.

blockage, as well as the obtention of a more hydrophobic surface that facilitates PO desorption, resulting in enhanced propylene conversion and PO yields.[29,31,32,34,38,40,46]

4. Conclusions

In summary, a simple and straightforward one-step process has been developed for the controlled deposition of gold nanoparticles of uniform diameter in a titanosilicate zeolitic surface through a direct anionic exchange (DAE) procedure, simultaneously introducing auxiliary mesoporosity in the framework and removing detrimental octahedral Ti species, exposing a larger amount of catalytically active tetrahedral Ti sites. The resulting hierarchic system addresses the main drawbacks encountered with these catalysts, such as diffusion issues and rapid deactivation, associated with their microporous nature. This way, the obtained Au_TS-1 catalyst displays an improved performance in the propylene epoxidation reaction along with outstanding stability typically challenging to achieve with these catalysts. Therefore, due to the exceptional performance of the developed catalyst and its extraordinarily simple preparation procedure without the need for a separate hierarchization step, we do believe that this material can have great relevance in industrial applications upon further optimization, paving the way for the design of new-generation materials that will be truly essential for the sustainable development of our society.

Author contributions

Ignacio Centeno-Vega: conceptualization, data curation, writing – original draft, writing – review & editing. Cristina Megías-Sayago: conceptualization, methodology, supervision, validation, writing – review & editing. Svetlana Ivanova: conceptualization, methodology, supervision, validation, writing – review & editing. Lorenzo José González Rubio: investigation, data curation, writing – original draft.

Data availability

Data for this article, including textural properties of the synthesized catalysts, calibration curves for the epoxidation products and catalytic activities are available at SienceDB at **https://www.scidb.cn/en/s/vQrM3m**.

Conflicts of interest

The authors declare that they have no known competing financial interests or personal relationships that could have appeared to influence the work reported in this paper.

Acknowledgements

I. Centeno-Vega would like to thank the Spanish Catalysis Society (SECAT) for the funding as part of the program of scholarships for the completion of a master's thesis in catalysis, as well as the Spanish Ministry of Science, Innovation and Universities for their support through an FPU grant (Ref. FPU23/00446). C. Megías-Sayago acknowledges the European Union's Horizon 2020 research and innovation programme for the funding received for this work under the Marie Skłodowska-Curie grant agreement no. 101022598.

References

1 Organisation for Economic Cooperation and Development (OECD), Global Plastics Outlook: Economic drivers, environmental impacts and policy options, 10.1787/de747aef-en, (accessed 17 June 2024).
2 M. Rabnawaz, I. Wyman, R. Auras and S. Cheng, *Green Chem.*, 2017, **19**, 4737–4753.
3 Organisation for Economic Cooperation and Development (OECD), Global Plastics Outlook: Policy Scenarios to 2060, 10.1787/aa1edf33-en, (accessed 17 June 2024).

4 P. Sahu, A. Thorbole and R. K. Gupta, *ACS Sustainable Chem. Eng.*, 2024, **12**(18), 6811–6826, DOI: 10.1021/acssuschemeng.4c01123.
5 G. Lopez, M. Artetxe, M. Amutio, J. Bilbao and M. Olazar, *Renewable Sustainable Energy Rev.* 73, 2017, 346–368, DOI: 10.1016/j.rser.2017.01.142.
6 A. Carniel, N. Ferreira dos Santos, F. S. Buarque, J. V. Mendes Resende, B. D. Ribeiro, I. M. Marrucho, M. A. Z. Coelho and A. M. Castro, *Green Chem.*, 2024, 26, 5708–5743, DOI: 10.1039/d4gc00528g.
7 Z. Terzopoulou, L. Papadopoulos, A. Zamboulis, D. G. Papageorgiou, G. Z. Papageorgiou and D. N. Bikiaris, *Polymers*, 2020, **12**(6), 1209, DOI: 10.3390/POLYM12061209.
8 K. Loos, R. Zhang, I. Pereira, B. Agostinho, H. Hu, D. Maniar, N. Sbirrazzuoli, A. J. D. Silvestre, N. Guigo and A. F. Sousa, *Front. Chem.*, 2020, **8**, 585, DOI: 10.3389/fchem.2020.00585.
9 H. Zhang, G. Zhou, M. Jiang, H. Zhang, H. Wang, Y. Wu and R. Wang, *Macromolecules*, 2020, **53**, 5475–5486.
10 S. K. Burgess, R. M. Kriegel and W. J. Koros, *Macromolecules*, 2015, **48**, 2184–2193.
11 N. M. Wang, G. Strong, V. Dasilva, L. Gao, R. Huacuja, I. A. Konstantinov, M. S. Rosen, A. J. Nett, S. Ewart, R. Geyer, S. L. Scott and D. Guironnet, *J. Am. Chem. Soc.*, 2022, **144**, 18526–18531.
12 R. J. Conk, S. Hanna, J. X. Shi, J. Yang, N. R. Ciccia, L. Qi, B. J. Bloomer, S. Heuvel, T. Wills, J. Su, A. T. Bell and J. F. Hartwig, *Science*, 2022, **377**, 1561–1566.
13 V. Farkas, P. Albrecht, Á. Erdélyi, M. Nagyházi, B. Csutorás, G. Turczel, N. Miskolczi, J. Bobek-Nagy, O. Osterthun, J. Klankermayer and R. Tuba, *Green Chem.*, 2024, **26**, 10225–10231.
14 R. J. Conk, J. F. Stahler, J. X. Shi, J. Yang, N. G. Lefton, J. N. Brunn, A. T. Bell and J. F. Hartwig, *Science*, 2024, **385**, 1322–1327.
15 X. Deng, Y. Wang, L. Shen, H. Wu, Y. Liu and M. He, *Ind. Eng. Chem. Res.*, 2013, **52**, 1190–1196.
16 S. Ivanova, C. Petit and V. Pitchon, *Appl. Catal., A*, 2004, **267**, 191–201.
17 C. Megías-Sayago, A. Lolli, S. Ivanova, S. Albonetti, F. Cavani and J. A. Odriozola, *Catal. Today*, 2019, **333**, 169–175.
18 C. Megías-Sayago, J. L. Santos, F. Ammari, M. Chenouf, S. Ivanova, M. A. Centeno and J. A. Odriozola, *Catal. Today*, 2018, **306**, 183–190.
19 M. Liu, Z. Huang, W. Wei, X. Wang and Y. Wen, *Front. Chem.*, 2021, **9**, 682404.
20 X. Feng, N. Sheng, Y. Liu, X. Chen, D. Chen, C. Yang and X. Zhou, *ACS Catal.*, 2017, **7**, 2668–2675.
21 H. Huang, J. Zheng, K. Wu, J. Lin, X. Lin, Q. Yao, Q. Fan, D. Wang, Y. Huang, J. Jiang and Z. Zheng, *J. Anal. Appl. Pyrolysis*, 2024, **182**, 106698.
22 Y. Zhu, J. Chen, W. Li, D. Wang, S. Li and Z. Zheng, *J. Anal. Appl. Pyrolysis*, 2020, **151**, 104906.
23 H. Ahmad Alyosef, H. Roggendorf, D. Schneider, A. Inayat, J. Welscher, W. Schwieger, T. Münster, G. Kloess, S. Ibrahim and D. Enke, *J. Porous Mater.*, 2016, **23**, 1609–1618.
24 A. Thangaraj, R. Kumar, S. P. Mirajkar and P. Ratnasamy, *Catalytic Properties of Crystalline Titanium Silicalites I. Synthesis and Characterization of Titanium-Rich Zeolites with MFI Structure*, 1991, vol. 130.
25 S. Krishnamurthy, A. Esterle, N. C. Sharma and S. V. Sahi, *Nanoscale Res. Lett.*, 2014, **9**, 627, DOI: 10.1186/1556-276X-9-627.
26 S. P. D. Ormond, M. Ratova, P. Kelly, M. Edge, B. Mihailova and L. Tosheva, *J. Porous Mater.*, 2016, **23**, 1421–1429.
27 W. S. Lee, M. Cem Akatay, E. A. Stach, F. H. Ribeiro and W. Nicholas Delgass, *J. Catal.*, 2012, **287**, 178–189.
28 M. Thommes, K. Kaneko, A. V. Neimark, J. P. Olivier, F. Rodriguez-Reinoso, J. Rouquerol and K. S. W. Sing, *Pure Appl. Chem.*, 2015, **87**, 1051–1069.
29 C. Du, N. Cui, L. Li, Z. Hua and J. Shi, *RSC Adv.*, 2019, **9**, 9694–9699.
30 G. Xiong, Q. Jia, Y. Cao, L. Liu and Z. Guo, *RSC Adv.*, 2017, **7**, 24046–24054.
31 Z. Jie, T. Yang, X. Wang, Y. Ji, Y. Li, B. Meng, X. Tan and S. Liu, *Surf. Interfaces*, 2022, **29**, 101741.
32 S. Karimi Haghighi and A. Nemati Kharat, *Inorg. Chem. Commun.*, 2021, **125**, 108413.
33 N. Sheng, D. Lin, W. Liang, C. Zhao, Y. Liu, Y. Zhu, Z. Song, J. Jiang, W. Xu, Z. Yang, B. Sun, X. Feng and C. Yang, *Chem. Eng. Sci.*, 2024, **300**, 120538.
34 T. Zhang, X. Chen, G. Chen, M. Chen, R. Bai, M. Jia and J. Yu, *J. Mater. Chem. A*, 2018, **6**, 9473–9479.
35 Y. Liu, C. Zhao, B. Sun, H. Zhu and W. Xu, *Appl. Catal., A*, 2021, **624**, 118329, DOI: 10.1016/j.apcata.2021.118329.
36 I. I. Ivanova and E. E. Knyazeva, *Chem. Soc. Rev.*, 2013, **42**, 3671–3688.
37 K. Zhu and X. Zhou, *Curr. Opin. Chem. Eng.*, 9, 2015, 42–48, DOI: 10.1016/j.coche.2015.07.009.
38 J. Yang, S. Liu, Y. Liu, L. Zhou, H. Wen, H. Wei, R. Shen, X. Wu, J. Jiang and B. Li, *iScience*, 2024, **27**(3), 109064, DOI: 10.1016/j.isci.2024.109064.
39 S. Shi, Y. Jing, Z. Zhang, W. Du, Y. Cao, X. Duan and X. Zhou, *Chem. Eng. J.*, 2024, **491**, 151732.
40 M. Lin, Z. Su and W. Ma, *Chem. Phys.*, 2024, **581**, 112259.
41 S. Ivanova, V. Pitchon and C. Petit, *J. Mol. Catal. A: Chem.*, 2006, **256**, 278–283.
42 G. Moretti, A. M. Salvi, M. R. Guascito and F. Langerame, *Surf. Interface Anal.*, 2004, **36**, 1402–1412.
43 D. Trong, L. Bonneviot, A. Bittar, A. Sayari and S. Kaliaguine, *Titanium sites in titanium silicalites: an XPS, XANES and EXAFS study*, 1992, vol. 74.
44 A. C. Alba-Rubio, J. L. G. Fierro, L. León-Reina, R. Mariscal, J. A. Dumesic and M. López Granados, *Appl. Catal., B*, 2017, **202**, 269–280.
45 J. Huang, C. Liu, D. Sun, Y. Hong, M. Du, T. Odoom-Wubah, W. Fang and Q. Li, *Chem. Eng. J.*, 2014, **235**, 215–223.
46 M. Lin, C. Xia, B. Zhu, H. Li and X. Shu, *Chem. Eng. J.*, 2016, **295**, 370–375.
47 Y. Li, Y. Yi, X. Wang, B. Gao, Y. Guo, G. Wu, Z. Feng and H. Guo, *Ind. Eng. Chem. Res.*, 2023, **62**, 12152–12173.
48 D. Liu, R. Wang, Y. Yu, Z. Chen, N. Fang, Y. Liu and M. He, *Catal. Sci. Technol.*, 2023, **13**, 1437–1447.

49 J. W. Harris, J. Arvay, G. Mitchell, W. N. Delgass and F. H. Ribeiro, *J. Catal.*, 2018, **365**, 105–114.
50 X. Feng, X. Duan, G. Qian, X. Zhou, D. Chen and W. Yuan, *Appl. Catal., B*, 2014, **150–151**, 396–401.
51 Z. Lu, J. Kunisch, Z. Gan, M. Bunian, T. Wu and Y. Lei, *ChemCatChem*, 2020, **12**, 5993–5999.
52 J. Huang, T. Takei, T. Akita, H. Ohashi and M. Haruta, *Appl. Catal., B*, 2010, **95**, 430–438.